

Lyapunov exponents from experimental time series. Application to cymbal vibrations

Cyril Touzé, Antoine Chaigne

▶ **To cite this version:**

Cyril Touzé, Antoine Chaigne. Lyapunov exponents from experimental time series. Application to cymbal vibrations. Acta Acustica united with Acustica, 2000, 86 (3), pp.557-567. hal-01134813

HAL Id: hal-01134813
https://ensta-paris.hal.science/hal-01134813

Submitted on 17 Nov 2017

HAL is a multi-disciplinary open access archive for the deposit and dissemination of scientific research documents, whether they are published or not. The documents may come from teaching and research institutions in France or abroad, or from public or private research centers.

L'archive ouverte pluridisciplinaire **HAL**, est destinée au dépôt et à la diffusion de documents scientifiques de niveau recherche, publiés ou non, émanant des établissements d'enseignement et de recherche français ou étrangers, des laboratoires publics ou privés.

Lyapunov Exponents from Experimental Time Series: Application to Cymbal Vibrations

Cyril Touzé, Antoine Chaigne
Ecole Nationale Supérieure des Télécommunications, Département TSI, CNRS URA 820, 46 Rue Barrault, 75634 Paris Cedex 13, France

Summary
Lyapunov exponents are among the most relevant and most informative invariants for detecting and quantifying chaos in a dynamical system. This method is applied here to the analysis of cymbal vibrations. The advantage of using a quadratic fit for determining the Jacobian of the dynamics is presented. In addition, the interest of using a time step for the evolution of the neighbourhood not equal to the timelag used for the reconstruction of the phase space is underlined. The robustness of the algorithm used yields a high degree of confidence in the characterization and in the quantification of the chaotic state.
To illustrate these features in the case of cymbal vibrations, transitions from quasiperiodicity to chaos are exhibited. The quasiperiodic state of the system is characterized together by the power spectrum of the experimental signal and by calculation of the Lyapunov spectrum.

1. Introduction

Cymbals belong to the category of nonlinear percussion instruments. In their normal use, these instruments are struck by a mallet. Pairs of cymbals can also be struck against each other, especially in bands or in orchestral use. Due to the rather heavy strokes, the vibrations of cymbals generally exhibit large amplitude, compared to their thickness, which leads to nonlinear effects. As a consequence, the pitch of such instruments is not clearly defined. Only at the end of the decay, as the magnitude of the motion becomes sufficiently small, one can clearly hear the most salient eigenfrequencies of the normal modes predicted by the linear theory. Previous investigations on cymbals are mostly concerned with the linear regime [1], and only a few references address the question of nonlinearity which is of prime importance for these instruments [2, 3]. In order to tackle this problem, one strategy consists in investigating the underlying physics of the vibrating structure. This method has been applied to gongs in the past [4, 5]. One complementary approach is to investigate the dynamical behaviour of these instruments with the help of nonlinear signal processing tools. This is the purpose of the present paper.

The main difficulty for the analysis of struck cymbals follows from the broadband excitation of the initial pulse. This pulse excites simultaneously a very large number of frequencies, in a very short amount of time, which makes it almost impossible to analyse the successive bifurcation mechanisms and the routes to chaos. In addition, the magnitude and location of the pulse is generally hard to reproduce. Therefore, it seems more appealing to drive the cymbal with slowly and continuously increasing magnitude, so that transitions from the linear to the chaotic state can be observed, and to limit the spectrum of the excitation. In practice, the cymbal is driven here sinusoidally at frequencies close to the most salient linear eigenfrequencies of the instrument, or intentionally apart from these eigenfrequencies [6]. The velocity of one selected point of the instrument is recorded during about three minutes (see Figure 5). At large amplitude, it is interesting to notice that the sound obtained by driving the cymbal with a sinusoid instead of a pulse is clearly comparable to characteristic cymbal sounds, although the tone quality may be somewhat poorer. This is a strong argument in favor of considering the typical sounds of the instrument in ordinary performances as a combination of the nonlinear effects due to a limited number of active modes.

In this paper, particular attention is paid to the calculation of the Lyapunov exponents from experimental time series. The method used here for computing the Lyapunov spectrum relies on an idea conjointly developped by Eckmann and Ruelle [7, 8] and Sano and Sawada [9]. This method consists of approximating the matrix of the linearized flow in the reconstructed tangent space. One major advantage of this method is that, in theory, the complete spectrum of the exponents can be obtained. Other methods, in which the divergence of nearby trajectories is used, are also possible candidates, but their principal limitation follows from the fact that, in practice, only the maximal exponent can be obtained [10, 11]. Other methods, based on a global reconstruction of the vector field and especially designed for short or noisy data sets, are also available [12, 13]. These methods will not be considered here.

The main features of the algorithm presented in this paper are the following: first, the local Jacobian of the evolution function in the reconstructed tangent space is approximated by a higher-order local polynomial [14, 15, 16]. As a consequence, it is expected that the accuracy in the determination of the negative exponents will be improved, and that the presence of spurious exponents, multiples of the true exponents, will be avoided. One example of the existence of such spurious exponents was first noted in [8]. More recently, an analytic proof has been given by Sauer et al. [17]. Second, a time step for the evolution of the neighbourhood is selected,

which is different from the timelag used for the reconstruction of the attractor. This improves significantly the determination of the exponents. These properties of the algorithm will be illustrated numerically on standard computer-generated time series originated from chaotic discrete and continuous dynamical systems.

Interpretation of the Lyapunov exponents related to real world data is a rather difficult task which should be done with great care. However, a number of successful applications can be mentioned, which cover various fields of physical systems: hydrodynamics [8], chemistry [10], fundamental physics [18, 19] and acoustics [20, 21], including musical acoustics [22, 23], and speech [24]. In section 3 of the paper, the computation of the Lyapunov exponents is applied to experimental time series obtained from measurements performed on a thin crash cymbal, which is driven sinusoidally at its center by means of a shaker. Similar experiments were conducted in the past by Fletcher, Rossing et al. [3, 5, 2]. By increasing slowly the amplitude of the shaker motion, transitions from linear to chaotic motion are observed. A complete description of the experimental setup can be found in [6], together with the results of the algorithms used for estimating the dimensions of the system (correlation dimension, and false nearest neighbours). The calculation of the Lyapunov exponents makes it possible to detect the presence of chaos, and to quantify the "degree of disorder" in the chaotic regime. In addition, this analysis gives us a better understanding on the route to chaos observed in the system, through testing of the quasiperiodicity of the measured signal. This point will be developed in section 4.

2. Calculation of the Lyapunov spectrum

2.1. Algorithm

The methods of current use in nonlinear signal processing are based on the Takens reconstruction theorem [25]. Recent surveys present both the theoretical background and applications of these techniques for chaotic signals [18, 19, 26]. Therefore, the fundations of this theory will not be developed further in this paper.

In order to compute the Lyapunov spectrum of a given time series, it is necessary to obtain the local Jacobian of the underlying flow from the trajectory in the reconstructed phase space. The principle is the following: Given a time series $\{s(n)\}_{n=1\ldots N}$, a multivariate trajectory is formed with a timelag T and a so-called embedding dimension d_E. The value of the timelag is usually taken as the first minimum of the Average Mutual Information function [27]. A lower bound for the embedding dimension can be given by using the test of the false nearest neighbours [28]. This yields the vector:

$$\mathbf{y}(k) = \Big[s(k), s(k+T), \ldots, s\big(k+(d_E-1)T\big)\Big].$$

Denoting $\mathbf{F}$ the evolution function which maps the vector $\mathbf{y}(k)$ onto the vector $\mathbf{y}(k+T_F)$, one can write:

$$\mathbf{y}(k+T_F) = \mathbf{F}\big(\mathbf{y}(k)\big), \tag{1}$$

where T_F is the time step for this local neighbourhood-to-neighbourhood mapping. The main task of the algorithm is to compute the local Jacobian matrix $\mathbf{DF}(k)$ in the tangent space, since the Lyapunov exponents are computed from the eigenvalues of the Jacobian.
Defining further:

- $\{\mathbf{y}(k_i)\}_{i=1\ldots N_v}$: the N_v nearest neighbours of $\mathbf{y}(k)$,
- $\boldsymbol{\eta}(k,i) = \mathbf{y}(k_i) - \mathbf{y}(k)$, $i = 1\ldots N_v$: the small displacements in the neighbourhood of $\mathbf{y}(k)$,
- $\boldsymbol{\eta}(k+T_F,i) = \mathbf{y}(k_i+T_F) - \mathbf{y}(k+T_F)$, $i = 1\ldots N_v$: the small displacements in the evolved neighbourhood, after T_F time steps,

the local Jacobian is then calculated via a Taylor expansion in equation (1). The standard method consists in linearizing $\mathbf{F}$, but it has been found that higher-order Taylor expansion give better results [16].

A second-order expansion, for example, with $i = 1\ldots N_v$, yields:

$$\boldsymbol{\eta}(k+T_F,i) = \mathbf{DF}(k)\boldsymbol{\eta}(k,i) + \frac{1}{2}\boldsymbol{\eta}(k,i)^t\mathbf{H}(k)\boldsymbol{\eta}(k,i) \tag{2}$$

where

$$\mathbf{DF}(k)_{i,j} = \left(\frac{\partial \mathbf{F}_i}{\partial \mathbf{y}_j}\right)\big(\mathbf{y}(k)\big)$$

is the Jacobian of the evolution function $\mathbf{F}$, and

$$\mathbf{H}(k)_{i,j,l} = \left(\frac{\partial^2 \mathbf{F}_i}{\partial \mathbf{y}_j \partial \mathbf{y}_l}\right)\big(\mathbf{y}(k)\big)$$

is the Hessian of $\mathbf{F}$.

Equation (2) is then projected onto a subspace of dimension $d_L \leq d_E$. d_L is the *local dimension* corresponding to the dimension of the manifold on which the dynamics takes place, which should not be mistaken for the embedding dimension d_E. The dimension d_E should be large enough so as to avoid the presence of false neighbours [18, 19]. All subsequent calculations are made in a d_L-dimension subspace, which provides us with d_L Lyapunov exponents.

The next step of the algorithm consists in calculating $\mathbf{DF}$ and $\mathbf{H}$ through matrix inversion corresponding to equation (2) (the Hessian part can be written in a matrix form. See, for example, [16] for more details). The coefficients of $\mathbf{H}$ are useful only for assessing the trajectory, since the Lyapunov spectrum is computed from the eigenvalues of $\mathbf{DF}$. Thus, only the Jacobian part is finally retained.

The last step of the algorithm is the classical QR decomposition of the Jacobian, which is evaluated along the phase space trajectory, in order to calculate the d_L Lyapunov exponents [7]. With K the number of points on the attractor for which the Jacobian has been estimated, $R_{(k)}$ the R matrix from the QR decomposition at $\mathbf{y}(k)$, and τ the sampling time step, the i^{th} Lyapunov exponent is given by:

$$\lambda_i = \frac{1}{\tau K T_F}\sum_{k=1}^{K}\ln\big(R_{(k)ii}\big).$$

This summary of the main steps of the algorithm shows that many parameters are involved: T and d_E for the reconstruction, T_F, d_L, K and N_v for the fit. For most of them, simple rules are clearly established to avoid pitfalls. A large number of references exist in the literature devoted to nonlinear signal processing where the rules for selecting appropriately these parameters are specified (see, for example, [18, 19, 29]).

2.2. Higher-order Taylor expansion

Most of the algorithms used for estimating the local Jacobian matrix restrict the Taylor expansion of equation (1) to the first-order (linear) term. In the present study, the use of higher-order expansions has been investigated. The major expected improvement is to increase significantly the accuracy of the results, especially for the negative exponents for which the linear algorithms present a number of difficulties [15, 16]. Two simultaneous burdens result from a linear fit on the Jacobian since, first, the trajectory must be approximated and, second, the Lyapunov exponents must be given. Using a higher-order expansion implies that all terms in the matrices of equation (2) are involved in the approximation of the local neighbourhood-to-neighbourhood mapping.

The accuracy of the results does not increase monotonically with the degree d_p of the expansion. This feature can be explained as follows: with increasing d_p, it is necessary to take a larger number of neighbours into account in order to perform the matrix inversion in good conditions. As a consequence, the assumption of small neighbourhood for the Taylor expansion is not verified any more. In other words, the number of selected neighbours N_v for computing the matrix must be large enough to overcome numerical instability, but, at the same time, this number is limited in order to keep the neighbourhood as small as possible. A good compromise consists in selecting N_v is given by [16]:

$$N_v = 2\left(\prod_{k=1}^{d_p}\frac{d_L+k}{k}-1\right).$$

Observations made by computing a third-order expansion of equation (1) show that the accuracy of the results is not significantly improved, compared to the second-order one. Therefore, it has been decided to select a second-order expansion.

Another important fact that justifies the use of a second-order expansion is linked to the problem of spurious exponents. One major problem, when dealing with experimental time series, is that the local dimension of the attractor, and thus the number of Lyapunov exponents, is not known. As a consequence, if the dimension is too large, then the algorithm presented in section 2.1 generates spurious exponents. With a first-order expansion, for a noise-free case, it is found that some of the spurious exponents are integer multiples of the true ones, as noted in [8] and demonstrated in [17].

With a second-order expansion, still for a noise-free case, the presence of those spurious exponents which are multiples of the true ones, is avoided. With a linear fit, a spurious exponent equal to twice the positive one appears as the local dimension d_L increases. This phenomenon may lead to the incorrect conclusion that two positive exponents exist in the system. By using a quadratic fit, those false multiple positive exponents are avoided. Despite our efforts, no analytical proof of this property could be given. Indeed, the mathematical derivations leading to the analytic result of [17], when extended to the quadratic case, give a system which bears an implicit solution [30]. However, a number of numerical calculations performed on different systems (Henon map, logistic map, Lorenz system) show that the quadratic fit eliminates the multiple spurious exponents. This feature is illustrated for the Henon map in Table I.

Table I. Calculated Lyapunov exponents for the Henon map, with linear and quadratic fits. The length of the sequence is equal to 40000 points, with $T = T_{FIT} = 1$ for a discrete map, $d_E = 8$ and K=1200. The apparition of a spurious exponent at twice the true positive one $\lambda_1 = 0.418$, with the linear fit, is clear. The second theoretical exponent is $\lambda_2 = -1.621$. With the quadratic fit, the spurious exponents are all negatives.

d_L	Lyapunov exponents, linear fit				
2	0.41468	-1.62298			
3	0.41585	-0.59021	-1.63580		
4	0.74228	0.40747	-1.58824	-1.86754	
5	0.82522	0.41393	-0.87694	-1.57883	-1.97449
d_L	Lyapunov exponents, quadratic fit				
2	0.41951	-1.62404			
3	0.42024	-0.87376	-1.62046		
4	0.41806	-0.48700	-0.87292	-1.62386	
5	0.41866	-0.31485	-0.44684	-0.86411	-1.61900

2.3. Selection of the evolution time T_F

Selecting an appropriate value for T_F is a particularly hard task in the case of continuous-time dynamical systems. Previous algorithms use $T_F = T$ as a general feature [8], because it substantially simplifies the implementation. However, there are no other justifications for this choice, and thus it is not recommended to select $T_F = T$, since there are no relations between these two quantities, as mentionned in [16]. The choice of T_F is directly connected to the choice of the discrete map which best fits the continuous flow, and no general rules are available for this problem.

However, for too small evolution time T_F, the local contraction or expansion properties of the flow are not well taken into account, thus leading to a bad estimate of the whole spectrum. On the contrary, when T_F approaches T, there is some probability for the trajectory to be too smoothed, hence leading to underestimate the negative exponents.

By studying the effect of T_F on a number of continuous maps, it has been observed that using a too small T_F leads to poor results, and that the precision of the estimated Lyapunov spectrum becomes acceptable as $T_F \geq T/2$. This feature is illustrated on a time series generated from the forced Duffing

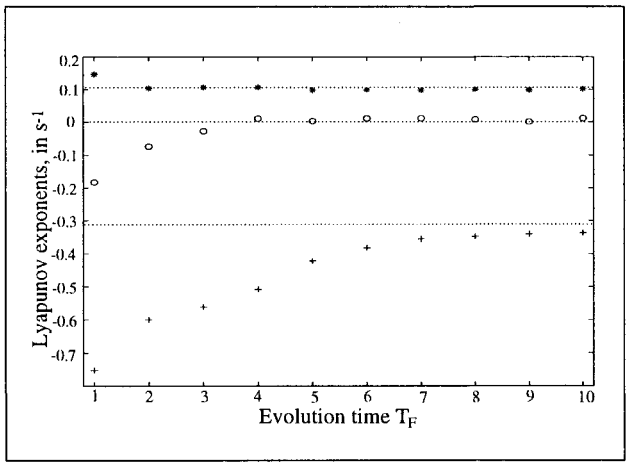


Figure 1. Lyapunov equation for the Duffing equation, as a function of the evolution time T_F. The parameters are K = 2000, T = 10, d_E= 6, and d_L = 3. 40000 points have been used for the calculation, with a quadratic fit. It can be seen that the acceptable values for the evolution time are obtained for $T_F \geq T/2$. The true exponent are marked by dotted lines.

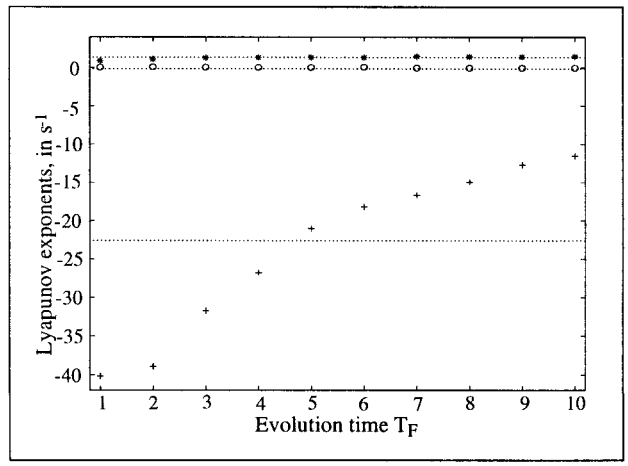


Figure 2. Lyapunov exponents for the Lorenz system, as a function of the evolution time T_F. The optimal value for T_F is $T/2$. The calculation has been made with 40000 points from the first coordinate of the Lorenz system, with K = 1500, d_E = 4, d_L = 3, and T =10. The true exponents are marked by dotted lines. A quadratic fit has been used. The influence of T_F is particularly visible on the negative exponent (marked by a (+)), whereas the positive one and the vanishing one ((*) and (o)) do not vary significantly with T_F.

equation:

$$\ddot{x} + \delta\dot{x} + x + x^3 = \alpha\cos(\omega t)$$

with $\delta = 0.2, \alpha = 40, \omega = 1$. For this choice of parameters, the Lyapunov exponents are $\lambda_1 = 0.11$, $\lambda_2 = 0$, $\lambda_3 = -0.31$ (in s^{-1}) [31]. The time series was calculated with initial conditions: $x = 1$ and $\dot{x} = 0.7$. The length of the series is equal to 40000 samples. The first 5000 samples were cut in order to avoid the influence of transients. A fourth-order Runge-Kutta method is applied to the system, with a sampling time step of 0.04 s. For this value, the first minimum of the Average Mutual Information function is obtained for $T = 10$ samples. In this example, Figure 1 shows that the best spectra are obtained for $T_F \geq T/2$. It has been found that this empirical rule remains valid for higher embedding dimensions.

In a second set of experiments, a time series obtained from the first coordinate of the Lorenz system, sampled by a fourth-order Runge-Kutta scheme, has been used. The sampling time step is equal to $\tau = 0.01$ s. In this case, the first minimum of the Averaged Mutual Information function is equal to 0.1 s, which corresponds to $T = 10$ samples. Figure 2 shows that in this case, the best spectrum is obtained for $T_F = T/2$.

In conclusion, it turns out that even if no general rule can be asserted, all particular cases investigated show that selecting $T_F \leq T/2$ leads to bad results.

2.4. Results on computer-generated time series

In order to check its validity and limits, the algorithm has been tested on computer-generated time series derived from well-known dynamical systems (logistic, Henon and Ikeda maps, Lorenz and Rossler systems, Duffing equation, superposition of two incommensurate sinusoids). In each situation,

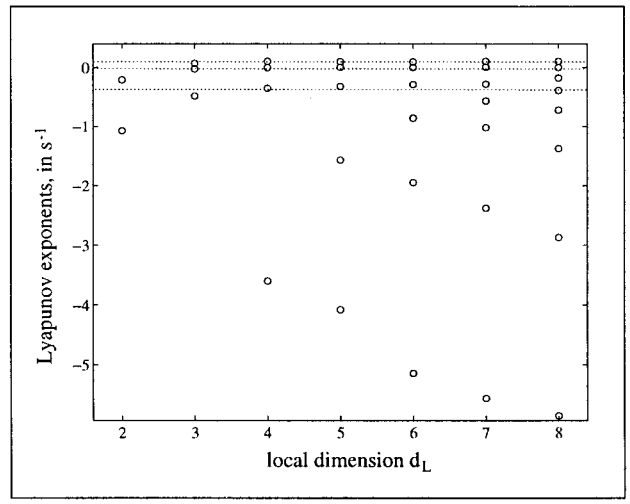


Figure 3. Lyapunov exponents for the Duffing equation as a function of the local dimension d_L, with K = 1400, T =10, T_F =6, d_E =8. The true exponents are marked with dotted lines.

a quadratic fit has been used. It is found that the true Lyapunov exponents are estimated within 1%. Only the two last examples (Duffing equations and incommensurate sinusoids) will be presented below. The first example is aimed at illustrating the performance of the method on a chaotic system, and the second example shows that the method used also yields excellent results with a non-chaotic signal.

Figure 3 shows the computed Lyapunov exponents for increasing values of d_L, with the time series used in the previous section. The evolution time is here T_F= 6 samples. The convergence of the true exponents (marked by dotted lines on Figure 3) with increasing d_L is clear, whereas the spurious ones vary with d_L. This can help in identifying the spuri-

ous exponents. This figure shows that the absolute value of the false exponents is systematically larger than the absolute value of the largest true one. However, this property cannot be generalized. Tests performed on the Lorenz system, for example, show that the spurious exponents obtained in this case are also all negatives, but that they are located between the vanishing exponent and the most negative one. These results are in accordance with those previously obtained by other authors [8, 16, 20, 32]. From these observations, one is led to conclude that it is not possible to exhibit a general rule for the location of the spurious numerical exponents in the Lyapunov spectrum.

A signal composed of two incommensurate audible frequencies has been also tested. The results show that the algorithm is robust for finding the two-torus on which the trajectory takes place, by exhibiting two clearly vanishing exponents whatever the local dimension d_L. The signal is made of the following frequencies: f_1 = 440 Hz and f_2 = $2\sqrt{2}f_1$ = 1244.5 Hz, with equal amplitudes. A trajectory of 40000 points has been used, with a sampling frequency F_e = 48000 Hz, a standard value for audio signals. The delay T for the reconstruction is equal to 16 samples. Figure 4 shows the convergence of the exponents, for a local dimension d_L equal to 3. The signature of a two-torus is assessed by the presence of two zero exponents, while the remaining ones are all negatives.

A commonly accepted method to discriminate the spurious exponents consists in computing the Lyapunov spectrum for a given time series, read first forward and then backward in time [31]. The expected behaviour is that the signs of the true exponents change with time reversal, whereas the spurious ones do not. This method has been found to give excellent results with time series issued from discrete maps (Henon, logistic and Ikeda map has been tested in this manner), thus leading to an undoubted identification of the spurious exponents. Unfortunately, in the case of continuous flows, the expected behaviour is not so clearly visible, and the identification of true and spurious exponents becomes slightly impossible. Thus, this method was not used in the present study.

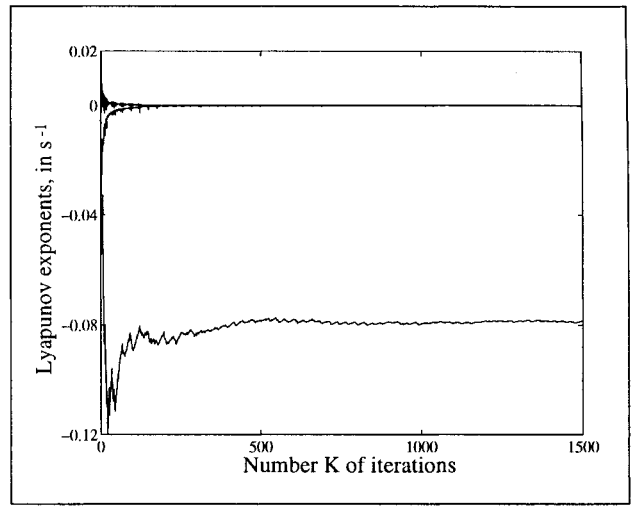


Figure 4. Convergence of the Lyapunov exponents with the number K of iterations for a signal composed by two incommensurate frequencies. The two first exponents are equal to zero, the third one (spurious) is negative, which is consistent with the theoretical results. The fixed parameters are: d_E = 6, d_L = 3, T = 16, T_F = 10.

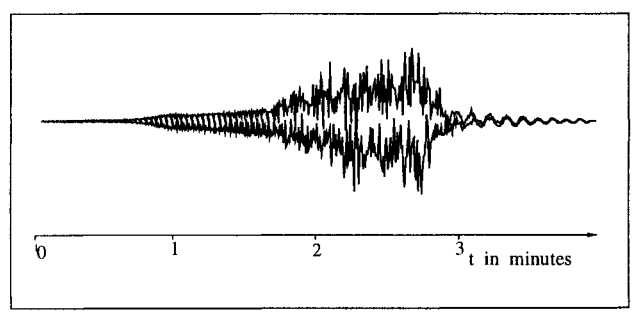


Figure 5. Global temporal shape of the signal recorded at the edge of the cymbal, with driving frequency F_{exc} = 412 Hz. The amplitude of the excitation is slowly and linearly increased until 2 min 40 s, time at which the driving force is suddenly removed.

3. Application to the cymbal

3.1. Experimental set-up

The previously described method for determining Lyapunov exponents has been applied to experimental time series on a Zildjian thin crash cymbal (diameter: 41 cm), in order to assess and quantify the chaotic regime. In this experiment, the cymbal is clamped at its center to an impedance head (B&K 8001) mounted on a LDS vibration exciter. The amplitude of the driving force is slowly and linearly increased by modulating the sinusoidal driving signal by a triangle waveform of very low frequency. The magnitude of the driving force lies within the range 1 to 20 N, depending on the driving frequency. The magnitude of the displacement at the edge is generally between 0.1 and 1 mm. However, this magnitude may become very large for some values of the excitation frequency. In certain cases, edge displacements up to 1 cm have been observed. The analyzed signal is delivered by an accelerometer (B&K 4393) glued either at the edge or at a distance of $r/2$ from the center, where r is the radius of the cymbal, and recorded on a DAT-tape with sampling frequency F_e = 48000 Hz. The duration of the recordings lies between 2 and 5 minutes. One example of recorded signal is shown in Figure 5. Sharp transitions can be seen on this figure, as well as the relaxation effect after suppression of the excitation, around t = 2 min 40 s. In order to observe various types of transitions, the forcing frequency is either close to one linear eigenfrequency of the cymbal, or significantly apart from eigenfrequencies and from low-order linear combinations of these frequencies. In a previous work, calculations of the correlation dimension and of the embedding dimension, by means of the false nearest neighbours method, have been performed on these signals. The results show, among other things, that the dimension of the underlying dynamics is less than or equal to 7 [6].

As it is generally the case for experimental signals, when compared to computer-generated series, for example, the present signals exhibit a finite signal-to-noise ratio (typically 50 dB). This signal-to-noise ratio is essentially due to the accelerometer. Moreover, the reconstruction does not display a clear fractal form. Since the algorithm makes extensive use of the geometrical properties of the phase portrait (neighbouring trajectories), some difficulties may be encountered in the determination of the exponents. To illustrate this, a two-dimensional reconstruction is shown in Figure 6, for a driving frequency F_{exc} = 526 Hz, after the onset of chaos.

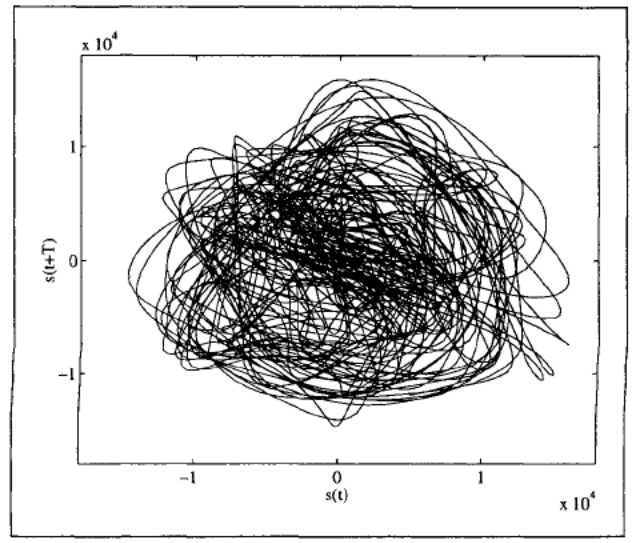


Figure 6. Trajectory in the reconstructed phase space, with T = 16, for an acceleration signal of the cymbal driven at 526 Hz, once the chaotic regime is established.

3.2. Results

The results presented below were obtained in the large amplitude vibration regime, characterized by a dense and broadband Fourier spectrum. In fact, one primary goal of this study was to assess that the cymbal vibration was really chaotic. Thus, the convergence of a positive Lyapunov exponent was expected. Calculations of the Lyapunov exponents were made for four different driving frequencies and for two different locations of the accelerometer. In each situation, a portion of 40000 points of the signal is selected (which corresponds to a duration of 0.83 s), once the chaotic regime is well established. In Figure 5, for example, a portion of 0.83 s was selected around 2mn30s. At that time, the driving force is typically equal to 10 N.

A typical curve of convergence is shown in Figure 7. This curve has been obtained for particular values of the involved set of parameters. It has been checked that the best convergence is obtained for T_F around $T/2$ as shown previously on calculated time series. It is observed that the convergence is less pronounced as T_F is equal to T. One can notice, in particular, the convergence of the largest exponent, for increasing values of d_L, which clearly indicates the presence of a p ositive exponent in the system. Thus, it can be concluded that the vibration is chaotic. One problem arising from the blurred trajectory of the experimental signal is that spurious exponents appear at positive, though relatively small, values.

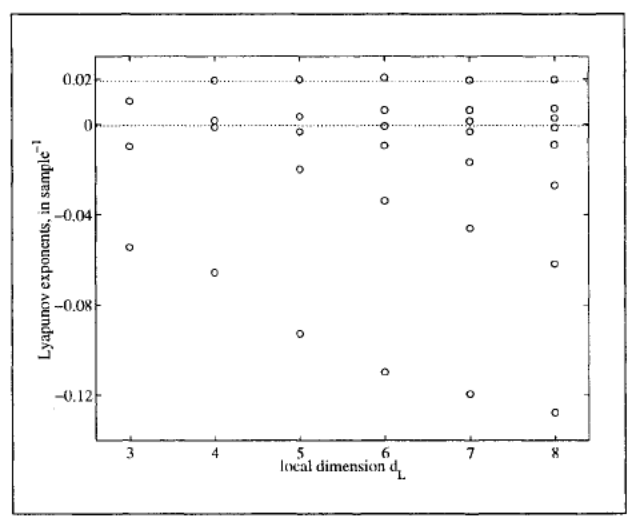


Figure 7. Lyapunov exponents in (sample)$^{-1}$, as a function of the local dimension d_L, for the acceleration signal recorded at the edge of the cymbal driven with F_{exc} = 526 Hz. 30000 points are used for the analysis. The parameters have the following values: d_E = 8, K = 2000, T = 16, T_F = 10. A clear convergence to 0.020 is observed for the largest exponent.

In order to validate the analysis, the results obtained are checked against theoretical rules given by different authors:

- The Kaplan-Yorke conjecture [33] yields a dimension d_{KY} from the spectrum of the Lyapunov exponents defined by:

$$d_{KY} = N + \frac{\sum_{i=1}^{N} \lambda_i}{|\lambda_{N+1}|}$$

  where N is such as : $\sum_{i=1}^{N} \lambda_i > 0$ and $\sum_{i=1}^{N+1} \lambda_i < 0$. This dimension d_{KY} can be used in comparison to the correlation dimension d_2 [34, 6] in order to get confidence in the calculated exponents. This also yields a guideline for the selection of the local dimension d_L.
- Theoretical results show that, when computing the Lyapunov spectrum from a time series derived from a continuous dynamical system, at least one vanishing exponent must be present which represents the continuity of the trajectory.

However, applications of theses rules show that one cannot conclude with absolute certainty on the validity of all Lyapunov exponents. Table II shows the results obtained for an acceleration signal recorded at the edge of the cymbal, with F_{exc} = 526 Hz. These results are also shown in Figure 7 for $d_L \in [3, 8]$. The correlation dimension for the same signal has already been calculated, which gives d_2 = 3.6 [6]. Comparing this value with d_{KY} calculated with the Lyapunov exponents shows that, for $d_L \geq 6$, d_{KY} becomes too large compared to d_2= 3.6. Thus, the best candidates for the spectrum are obtained for d_L equal to 4 or 5. At this stage, it cannot be concluded with certainty which of these two spec-

Table II. Calculated Lyapunov exponents for three different values of the local dimension d_L, for the cymbal driven at 526 Hz, and with the acceleration measured at the edge. The length of the experimental sequence is equal to 40000 points. The other fixed parameters are: $d_E = 8$, $T = 16$, $T_F = 10$, $K = 2000$. The exponents are given here in normalized units with respect to the sampling time, i.e. in sample^{-1}.

d_L	Lyapunov exponents (in sample^{-1})						d_{KY}
4	0.01936	0.00157	-0.00130	-0.06571			3.12
5	0.01979	0.00349	-0.00334	-0.01989	-0.09271		4.02
6	0.02060	0.00625	-0.00088	-0.00938	-0.03393	-0.10969	4.55

Table III. Calculated Lyapunov exponents in sample^{-1} for the cymbal driven at 412 Hz, with a time series of 40000 points. The fixed parameters are: $d_E = 8$, $T = 10$, $T_F = 8$, $K = 2000$.

d_L	Lyapunov exponents (in sample^{-1})					d_{KY}
4	0.02325	0.00001	-0.01779	-0.08425		3.06
5	0.02457	0.00636	-0.00582	-0.02460	-0.09147	4.02

Table IV. Correlation dimension d_2, embedding dimension d_E and greatest Lyapunov exponents λ, in (ms)$^{-1}$, for four different driving frequencies. Each Lyapunov exponent calculation has been made with a time series of 40000 points, using a quadratic fit.

F_{exc} (Hz)	Recording Position	d_2	d_E	λ (ms)$^{-1}$
412	r/2	3,4	5	$1,15 \pm 0.01$
412	edge	2,9	5	0.82 ± 0.02
440	r/2	3,8	5	$1,38 \pm 0.02$
526	edge	3,6	5	$0,94 \pm 0.01$
385	edge	4,6	7	$0,75 \pm 0.01$
385	r/2	4,5	6	1.42 ± 0.06

tra is the most valid. A similar discussion can be made for $F_{exc} = 412$ Hz. Table III shows the results for $d_L = 4$ and 5, which are here also the best possible candidates. Application of the rule related to the p resence or not of a vanishing exponent in the spectrum could lead to the conclusion that the exponents obtained with $d_L = 4$ are right. However, the correlation dimension of this signal is equal to 3.4, and thus the Lyapunov spectrum calculated with $d_L = 5$ cannot be completely rejected.

In view of the results obtained in the two typical cases presented in Table II and in Table III, one can be confident in the estimation of the largest exponent but not in the relevance of the other exponents in the spectrum. For these reasons, it has been decided to limit the present analysis to the convergence of the largest exponent.

The results obtained for four different driving frequencies are summarized in Table IV, together with the correlation dimension d_2 and the minimum embedding dimension d_E to use, given by the false nearest neighbours. This Table shows that a positive Lyapunov exponent has been found in each case, which is certainly the strongest indication that the system really exhibits chaos, since the calculation of Lyapunov exponent is more reliable than the correlation dimension. The precision given in this Table for the largest Lyapunov exponent is just the stan dard deviation calculated on the last 1000 iterations. The calculations are made typically with $K \in [1500, 2500]$ iterations, and the convergence is obtained in less than 1000 iterations. Figure 4 shows an example for a theoretical case (two incommensurate frequencies), where it turns out that 1500 iterations are largely sufficient for the convergence. Finally, it can be noticed in Table IV that the exponents are of the same order of magnitude for all different driving frequencies.

4. Route to chaos

4.1. Ruelle-Takens theory

In this section, attention is paid to the characterization of experimental transition scenarii from quasiperiodicity to chaos observed in the vibrations of the cymbal submitted to sinusoidal driving force with increasing amplitude. Calculation of the Lyapunov spectrum during the transition, as well as power spectrum analysis, are used for identifying the route to chaos observed. This section starts with a brief survey on the Ruelle-Takens theory. The interested reader is referred to dedicated references for a complete description of the most classical routes to chaos and of their general properties (see, for example, [35, 36]). Specific routes to chaos (such as period doubling, quasiperiodicity, intermittencies, crises,...) have been extensively studied in the past, on both theoretical and experimental viewpoints. These routes show, in particular, that the underlying mechanisms are governed by some universal laws. In this context, the Ruelle-Takens theory postulates that a limited number of Hopf bifurcations are involved in the transition from a stationary state to a chaotic state, for any physical system [37, 38]. In other words, this theory establishes that, if a system exhibits three Hopf bifurcations, then there is high probability for this system to be chaotic with a strange attractor.

Table V. Calculated Lyapunov exponents before the onset of chaos, for the cymbal driven at F_{exc} = 440 Hz. The acceleration is measured at r/2. The presence of two vanishing exponents is clearly observed (the first two ones), indicating the presence of a two-torus. The motion is quasiperiodic.

d_L	Lyapunov exponents (in sample^{-1})					
2	0.00034	-0.01823				
3	0.00104	0.00006	-0.11245			
4	0.00095	-0.00025	-0.04235	-0.14653		
5	0.00063	-0.00032	-0.03498	-0.07654	-0.17654	
6	0.00039	-0.00014	-0.02134	-0.04657	-0.08675	-0.18659

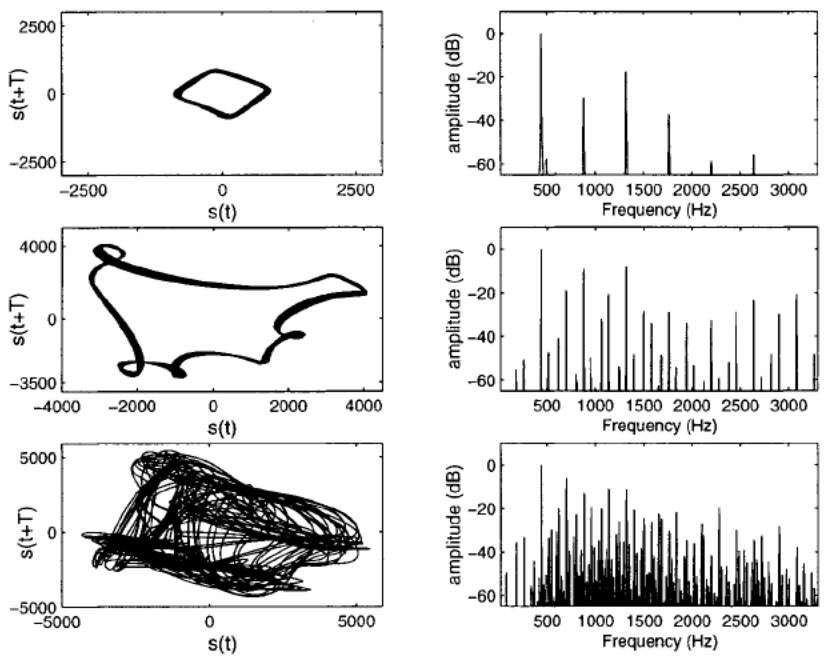


Figure 8. Reconstructed trajectory and power spectrum at three successive instants of time, showing three typical phases of the transition to chaos. The cymbal is driven at F_{exc} = 440 Hz and the acceleration is recorded at $r/2$.

In physical systems, the following characteristic features are thus expected, as the control parameter of the system increases (in our case, the magnitude of the driving force): Initially, The power spectrum of the observed variable (here, the acceleration of a given point on the cymbal) shows one peak at a given frequency f_1 (plus, eventually, some harmonics). The phase portrait will be a simple closed curve, the Lyapunov spectrum will display a single zero exponent, the other ones being negatives. Then, after a first Hopf bifurcation, the Fourier spectrum is made of two frequencies f_1 and f_2, and, in addition, of all combinations $f = m_1 f_1 + m_2 f_2$, with $(m_1, m_2) \in \boldsymbol{Z}^2$. The phase space trajectory is located on a two-torus. At this stage, one should make a clear distinction between two cases. The first case corresponds to mode locking which occurs when the ratio between the two frequencies f_1 and f_2 is rational. As a consequence, the trajectory on the torus will close itself after a finite number of cycles. In the second situation, the ratio between these two frequencies is irrational: the frequencies are incommensurate, and thus the torus is densely covered by the trajectory which never closes itself. In this case, the Lyapunov spectrum exhibits clearly two zero exponents. When the third Hopf bifurcation is about to appear, the phase portrait shows typical foldings, indicating that the two-torus will be destroyed, and hence that the system will gain an additional dimension [39, 40]. If another Hopf bifurcation arises (i.e. if a third frequency f_3 is to appear in the power spectrum), then a "broad-band noise", which is characteristic of chaos, is observed, and the torus breaks up in favor of a strange attractor. It will be shown in the next section that the experimental signals recorded on the cymbal show, to variable extent, all the abovementioned characteristics.

A clear survey of the transition scenarii can be found in [35]. Details on the quasiperiodicity routes to chaos are studied in [41, 42].

4.2. Mode-locking and quasiperiodicity

Figure 8 shows the phase portrait and the power spectrum of the acceleration signal recorded on the cymbal at $r/2$, at three successive instants of time. The driving frequency is F_{exc} = 440 Hz. In the first raw of the figure, the vibratory motion of

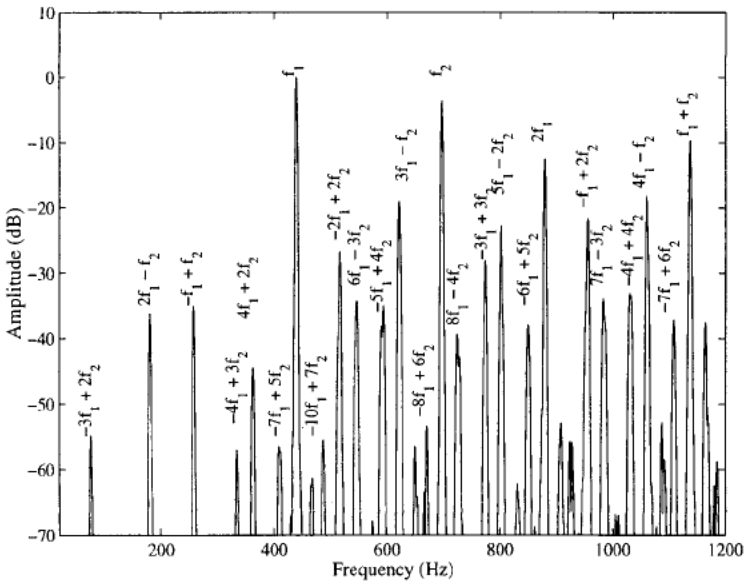


Figure 9. Power spectrum of the previous signal below 1200 Hz during the quasiperiodic state, with F_{exc} = 440 Hz. All frequency peaks can be written as linear combination of $f_1 = F_{exc}$ and f_2 = 698 Hz, where f_2 corresponds to one eigenfrequency of the cymbal.

the cymbal is weakly nonlinear. The power spectrum shows a peak at $f = F_{exc}$, and some harmonics. The reconstructed trajectory is a simple closed loop. The Lyapunov spectrum exhibits one vanishing exponent ($\lambda = 0.0 \pm 10^{-4}$, corresponding to the continuity of the flow), the other ones being negatives. By increasing the amplitude of the driving force, a Hopf bifurcation occurs. Therefore, a second frequency and combinations between F_{exc} and this new frequency become visible. The motion is quasiperiodic. The phase portrait displays typical foldings indicating that the trajectory is located on a two-torus which is about to be destroyed. With increasing amplitude, a second bifurcation is observed, and a broadband spectrum indicates the onset of chaos, as it can be seen on the phase portrait also.

A zoom on the low-frequency part of the power spectrum in the quasiperiodic state is shown in Figure 9. The identification of a quasiperiodic motion can be made here by noticing that all frequency peaks, in this part of the spectrum, can be written as the combination $f = m_1 f_1 + m_2 f_2$, with $f_1 = F_{exc} = 440$ Hz, and another fixed frequency f_2 = 698 Hz. This frequency f_2 corresponds here to one particular eigenfrequency of the cymbal. This result is in accordance with one possible interpretation of the Ruelle-Takens scenario presented in [36]: the Hopf bifurcation occurs when one mode of the system is destabilized and becomes active (ie the real part of the eigenvalue of this eigenmode becomes positive). The vibratory motion is then governed by two incommensurate frequencies. Calculations of the Lyapunov exponents were made just before the onset of chaos. The Lyapunov spectrum clearly displays two vanishing exponents (see Table V). This indicates that the trajectory is located on a manifold topologically equivalent to a two-torus and confirms that the transition to chaos is obtained by the break-up of a two-torus. If another eigenfrequency becomes active with increasing amplitude, then the motion becomes chaotic, as shown in the last raw of Figure 8, and as has been shown by the presence of one positive Lyapunov exponent (see section 3).

Similar observations and calculations were made for other driving frequencies, for which there is no evident relationship with the eigenfrequencies of the cymbal (F_{exc} = 412, 526 and 385 Hz have been tested). Moreover, experiments at a fixed level of excitation (which is sufficient to reach the quasiperiodic state), and with slight variations of the excitation frequency, have been conducted. Hysteresis cycles were clearly observed, with different resonance curves, depending on F_{exc} is increased or decreased.

Finally, some experiments were conducted with a driving frequency equal to twice one particular eigenfrequency of the cymbal. In this case, as expected, the following behaviour is observed: a mode-locking occurs between F_{exc} and the eigenfrequency defined by $f_\alpha = F_{exc}/2$. This result can be seen in Figure 10, where the driving frequency is F_{exc} = 248 Hz, and the eigenfrequency corresponding to the (4,0) mode of the cymbal is 124 Hz. An energy transfer from the low-frequency to the high-frequency range is clearly visible in the power spectrum shown in figure 10. Here, the motion is phase-locked in a ratio 2:1. As the amplitude of the forcing frequency increases, the system suddenly changes to chaotic behaviour which is characterized by a positive Lyapunov exponent, as it has been shown in Section 3 ($\lambda = 0.3 \pm 0.1$ $(\text{ms})^{-1}$. This value was not reported in table IV because the recorded signal was to short to yield sufficient accuracy to be extremely confident in the result). This result suggests that the system is structurally unstable after the second Hopf Bifurcation, and that no quasiperiodicity involving three different frequencies occurs. With increasing amplitude of the driving force, the two-torus directly breaks up in favor of a strange attractor.

In conclusion, the whole set of analysis tools used for characterizing the transition scenario (Fourier and Lyapunov spectrum, phase portrait) indicates that the main features of a

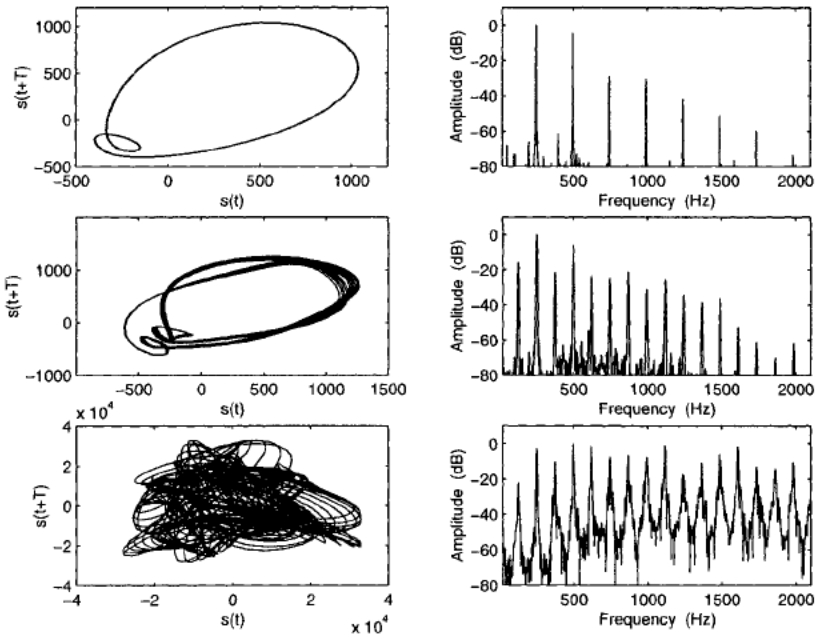


Figure 10. Reconstructed trajectory and power spectrum of the acceleration signal at three successive instants of time, with F_{exc} = 248 Hz. The eigenfrequency of mode (4,0) is at 124 Hz. It can be seen that the motion is phase-locked after the first Hopf bifurcation. By increasing the amplitude of the driving frequency, the motion becomes chaotic.

Ruelle-Takens scenario are present. However, at this stage of the work, the number of analyzed signals is limited, and thus no global laws such as the Farey tree at the onset of chaos [41, 42], can be clearly exhibited.

5. Conclusion

In this paper, a study on the vibratory motion of a cymbal has been presented, using nonlinear signal processing tools. Special emphasis has been put on the computation of the Lyapunov exponents from experimental time series, since it is one of the most reliable and most relevant invariant in order to detect and quantify chaos. In this context, an algorithm for estimating the Lyapunov spectrum has been developed. Specific features were used for improving the quality of the estimation. First, a second-order Taylor expansion has been used in order to improve the accuracy with which the exponents are given. It has been shown numerically that this quadratic fit avoids the presence of spurious exponents which are multiples of the true ones. Second, a time step for the evolution of the neighbourhood, which is different from the time step used for the reconstruction, has been selected. This also improves the accuracy of the results.

The ability of the method has been clearly shown on theoretical time series. In the case of experimental time series, only the largest Lyapunov exponent has been clearly exhibited, like it is most often the case in adverse experimental context.

The calculations of the Lyapunov exponents were made before the chaotic regime. This yields additional arguments for the identification of the observed transition scenario. The exponents, together with the observation of spectral peaks combinations, allows clear confidence in the fact that the system is subjected to a transition from quasiperiodicity to chaos. Depending on the value of the driving frequency, mode-locking and quasiperiodic states have been observed, as well as the succession of two Hopf bifurcations from the linear to the chaotic vibration.

The following general features of the phenomena have been underlined. First, a mode-locking is observed in the case of a driving frequency equal to twice the value of one particular eigenfrequency of the cymbal. Second, a quasiperiodicity is observed for other driving frequencies. This quasiperiodicity is associated to the combination of spectral peaks and to typical foldings of the trajectory in the phase space. In this case, the presence of two vanishing exponents in the Lyapunov spectrum indicates the presence of a two-torus.

When the amplitude of the forcing frequency increases, the two-torus breaks in favor of a strange attractor, whose presence is clearly identified by a positive Lyapunov exponent. This completes the description of the transition scenario for the cymbal, and quantifies the chaotic regime in terms of magnitude of the largest Lyapunov exponent.

Acknowledgement

The authors would like to thank Paul Manneville and Olivier Michel for fruitful discussions related to the physics of the system, and to nonlinear signal processing problems. We also wish to thank David Ruelle for giving favourable consideration to the problem of the spurious exponents which are multiples of the true ones, and Denis Matignon for his help in some tedious calculations. Many thanks also to Staffan Schedin for his contribution in the experimental part of the work.

References

[1] T. D. Rossing, R. B. Sheperd: Acoustics of cymbals. Proceedings of the 11th ICA, Paris, 1983. 329–333.

[2] C. Wilbur, T. D. Rossing: Subharmonic generation in cymbals at large amplitude. J. Acoust. Soc. Am. **101** (1997) 3144. Pt.2.

[3] N. H. Fletcher: Nonlinear dynamics and chaos in musical instruments. – In: Complex systems: from biology to computation. D. Green, T. Bossomaier (eds.). IOS Press, Amsterdam, 1993, 106–117.

[4] N. H. Fletcher: Nonlinear frequency shifts in quasispherical-cap shells: pitch glide in chinese gongs. J. Acoust. Soc. Am. **78** (1985) 2069–2073.

[5] K. A. Legge, N. H. Fletcher: Nonlinearity, chaos, and the sound of shallow gongs. J. Acoust. Soc. Am. **86** (1989) 2439–2443.

[6] C. Touzé, A. Chaigne, T. Rossing, S. Schedin: Analysis of cymbal vibration using nonlinear signal processing tools. Proceedings of ISMA 98, Leavenworth, 1998. 377–382.

[7] J. P. Eckmann, D. Ruelle: Ergodic theory of chaos and strange attractors. Reviews of modern Physics **57** (1985) 617–656.

[8] J. P. Eckmann, S. O. Kamphorst, D. Ruelle, S. Ciliberto: Liapunov exponents from time series. Physical Review A **34** (1986) 4971–4979.

[9] M. Sano, Y. Sawada: Measurements of the Lyapunov spectrum from chaotic time series. Phys. Rev. Letters **55** (1985) 1082.

[10] A. Wolf, J. B. Swift, H. L. Swinney, J. A. Vastano: Determining Lyapunov exponents from a time series. Physica D **16** (1985) 285–317.

[11] H. Kantz: A robust method to estimate the maximal Lyapunov exponents of a time series. Physics Letters A **185** (1994) 77–87.

[12] J. B. Kadtke, J. Brush, J. Holzfuss: Global dynamical equations and Lyapunov exponents from noisy chaotic time series. Int. J. of Bif. and Chaos **3** (1993) 607–616.

[13] R. Brown: Calculating Lyapunov exponents for short and/or noisy data sets. Physical Review E **47** (1993) 3962–3969.

[14] P. Bryant, R. Brown, H. Abarbanel: Lyapunov exponents from observed time series. Phys. Rev. Letters **65** (1990) 1523–1526.

[15] K. Briggs: An improved method for estimating Liapunov exponents of chaotic time series. Physics Letters A **151** (1990) 27–32.

[16] R. Brown, P. Bryant, H. Abarbanel: Computing the Lyapunov spectrum of a dynamical system from an observed time series. Physical Review A **43** (1991) 2787–2806.

[17] T. D. Sauer, J. A. Tempkin, J. A. Yorke: Spurious Lyapunov exponents in attractor reconstruction. Phys. Rev. Letters **81** (1998) 4341–4344.

[18] H. D. I. Abarbanel: Analysis of observed chaotic data. Springer, New-York, 1996.

[19] H. Kantz, T. Schreiber: Nonlinear time series analysis. Cambridge University Press, Cambridge, 1997.

[20] J. Holzfuss, W. Lauterborn: Liapunov exponents from a time series of acoustic chaos. Physical Review A **39** (1989) 2146–2152.

[21] T. W. Frison, H. D. I. Abarbanel, J. Cembrola, B. Neales: Chaos in ocean ambient noise. J. Acoust. Soc. Am. **99** (1996) 1527–1539.

[22] T. D. Wilson, D. H. Keefe: Characterizing the clarinet tone: Measurements of Lyapunov exponents, correlation dimension, and unsteadiness. J. Acoust. Soc. Am. **104** (1998) 550–561.

[23] M. H. Lee, J. N. Lee, K. Soh: Chaos in segments from Korean traditional singing and Western singing. J. Acoust. Soc. Am. **103** (1998) 1175–1182.

[24] M. Banbrook, G. Ushaw, S. McLaughlin: How to extract Lyapunov exponents from short and noisy time series. IEEE Transactions on Signal Processing **45** (1997) 1378.

[25] F. Takens: Detecting strange attractors in turbulence. Springer ed. Warwick, 1981, 366. in D. Rand and L.S. Young editors.

[26] E.Ott, T. Sauer, J. Yorke: Coping with chaos: Analysis of chaotic data and the exploitation of chaotic systems. Wiley Interscience, New-York, 1994.

[27] A. M. Fraser, H. L. Swinney: Independant coordinates for strange attractors from mutual information. Physical Review A **33** (1986) 1134–1140.

[28] M. B. Kennel, R. Brown, H. D. I. Abarbanel: Determining embedding dimension for phase-space reconstruction using a geometrical construction. Phys. Rev. A **45** (1992) 3403–3411.

[29] P. Grassberger, T. Schreiber, C. Schaffrath: Nonlinear time sequence analysis. Int. J. of Bif. and Chaos **1** (1991) 521–547.

[30] C. Touzé, D. Matignon: Techniques d'ordre supérieur pour l'élimination d'exposants de Lyapunov fallacieux. Rencontres du Non-linéaire 2000, Mars 2000.

[31] U. Parlitz: Identification of true and spurious Lyapunov exponents from time series. Int. J. of Bif. and Chaos **2** (1992) 155–165.

[32] R. Stoop, J. Parisi: Calculation of Lyapunov exponents avoiding spurious elements. Physica D **50** (1991) 89–94.

[33] J. L. Kaplan, J. A. Yorke: Chaotic behaviour in multidimensional difference equations. – In: Functional differential equations and approximation of fixed points. H. Peitgen, H. Walter (eds.). Springer, Berlin, 1979, 204–227.

[34] P. Grassberger, I. Procaccia: Measuring the strangeness of strange attractors. Physica D **9** (1983) 189–208.

[35] H. G. Schuster: Deterministic chaos. 3rd augmented edition ed. VCH, Weinheim, 1995.

[36] P. Manneville: Structures dissipatives, chaos et turbulence. Collection Aléa-Saclay ed. Academic Press, 1991.

[37] D. Ruelle, F. Takens: On the nature of turbulence. Communications in Mathematical Physics **20** (1971) 167.

[38] S. Newhouse, D. Ruelle, F. Takens: Occurrence of axiom-A attractors near quasi-periodic flows on T^m, $m \geq 3$. Communications in Mathematical Physics **64** (1978) 35.

[39] P. Bergé, Y. Pomeau, C. Vidal: L'ordre dans le chaos. Hermann, Paris, 1984.

[40] J. H. Curry, J. A. Yorke: A transition from Hopf bifuraction to chaos. Lect. Notes in Math. **668** (1978). Springer, New-York.

[41] M. H. Jensen, P. Bak, T. Bohr: Transition to chaos by interaction of resonances in dissipative systems. I. circle maps. Physical review A **30** (1984) 1960–1969.

[42] T. Bohr, P. Bak, M. H. Jensen: Transition to chaos by interaction of resonances in dissipative systems. II. Josephson junctions, charge-density waves, and standard maps. Physical review A **30** (1984) 1970–1981.